

Efficient Multi-agent Navigation with Lightweight DRL Policy

The International Journal of Robotics Research
 XX(X):1–11
 ©The Author(s) 2024
 Reprints and permission:
 sagepub.co.uk/journalsPermissions.nav
 DOI: 10.1177/ToBeAssigned
 www.sagepub.com/

SAGE

Xingrong Diao¹ and Jiankun Wang^{1,2}

Abstract

In this article, we present an end-to-end collision avoidance policy based on deep reinforcement learning (DRL) for multi-agent systems, demonstrating encouraging outcomes in real-world applications. In particular, our policy calculates the control commands of the agent based on the raw LiDAR observation. In addition, the number of parameters of the proposed basic model is 140,000, and the size of the parameter file is 3.5 MB, which allows the robot to calculate the actions from the CPU alone. We propose a multi-agent training platform based on a physics-based simulator to further bridge the gap between simulation and the real world. The policy is trained on a policy-gradients-based RL algorithm in a dense and messy training environment. A novel reward function is introduced to address the issue of agents choosing suboptimal actions in some common scenarios. Although the data used for training is exclusively from the simulation platform, the policy can be successfully transferred and deployed in real-world robots. Finally, our policy effectively responds to intentional obstructions and avoids collisions. The website is available at <https://sites.google.com/view/xingrong2024efficient/%E9%A6%96%E9%A1%B5>.

Keywords

Multi-agent systems, distributed collision avoidance, reactive and sensor-based planning, simulation to real gap.

1 Introduction

Multi-agent systems are increasingly used in robotics and artificial intelligence, such as industrial automation (e.g.,), material transportation (e.g., Xie et al. (2024)), and agricultural automation (e.g., Dutta et al. (2021)). The main challenge is implementing an efficient, robust, and safe navigation algorithm for multiple robots so that the robot can safely and efficiently complete point-to-point movement.

The traditional approaches for solving the problem of multi-agent navigation are primarily categorized into two types. One of the approaches is the centralized approach. These approaches calculate trajectories for each agent through a central server using the state of all agents and their respective workspaces (e.g., Tang et al. (2018), Zhou et al. (2021)). However, the computational cost associated with these approaches escalates as the number of agents increases, along with the maintenance of a more extensive communication network. In addition, once the central server is attacked, all agents will stop working. The other approach is the decentralized approach, which is deployed to each agent, empowering them with the capability to make decisions (e.g., Reciprocal Velocity Obstacle (RVO, Fiorini and Shiller (1998)), Optimal Reciprocal Collision Avoidance (ORCA, van den Berg et al. (2011))). However, these algorithms rely on a perfect perception of the environment and the state of the other agents, posing challenges for their application in larger-scale scenarios and deployment onto real-world robots. Numerous variants have been proposed to address these limitations (e.g., Alonso-Mora et al. (2010), Godoy et al. (2016)). Additionally, RVO and its variants often necessitate tuning numerous hyperparameters

to achieve optimal performance, and the adjustment of these parameters is highly dependent on the specific scenario.

Learning-based approaches have been proposed for robot navigation in recent years. Some approaches use imitation learning to learn from expert data and work successfully (e.g., Karnan et al. (2022), Yan et al. (2023)). However, the effectiveness of imitation learning depends on expert data quality, and it is challenging to handle scenarios out of the expert data. Other approaches employ reinforcement learning (RL) or deep reinforcement learning (DRL) to train policy. Some RL-based approaches achieve desired outcomes by modifying the reward function (e.g., Xie and Dames (2023), Han et al. (2022)). These approaches can yield great results in corresponding scenarios, but some suffer from overly redundant reward function designs and struggle to handle unforeseen scenarios. Some approaches train agents in specific scenarios to learn more diverse policies (e.g., Fan et al. (2020), Xue and Chen (2024)). Learning in more specific scenarios can enrich policies but demands higher standards for scenario design. Besides, there are efforts to bridge the gap between simulation and the real world by using progressive networks or adding randomness to the simulator (e.g., Rusu et al. (2016), Xie et al. (2023)).

¹Shenzhen Key Laboratory of Robotics Perception and Intelligence, Department of Electronic and Electrical Engineering, Southern University of Science and Technology, Shenzhen 518055, China.

²Jiaying Research Institute, Southern University of Science and Technology, Jiaying 314000, China.

Corresponding author:

Jiankun Wang.

Email: wangjk@sustech.edu.cn

Such approaches enable better deployment of policies learned from simulators on real robots, yet they do not fully leverage physics-based simulators. Finally, as the robot in a decentralized system can only perceive local observations during navigation, the decentralized robot navigation can be defined as the partially observable Markov decision process (POMDP). Most policies use convolutional neural networks (CNN) to encode perceptual information (e.g., [Liu et al. \(2020\)](#), [Chen et al. \(2020\)](#)), which results in the loss of historical information during navigation. Some approaches propose using Long Short-Term Memory (LSTM, [Hochreiter and Schmidhuber \(1997\)](#)) to record memory, providing more comprehensive information for navigation (e.g., [Liu et al. \(2021\)](#), [Cui et al. \(2022\)](#)).

In this paper, we propose a lightweight end-to-end distributed multi-agent navigation policy that maps raw LiDAR observation into action commands for the agents. We use the LiDAR sensor in perception for the following reasons ([Zhu and Zhang \(2021\)](#)): 1. the gap of the LiDAR sensor between the simulation and the real world is close; 2. the small measurement dimension of LiDAR is beneficial for simulation-to-real transfer. Furthermore, we introduce a physics-based simulation platform tailored for multi-agent training to bridge the gap between simulation and the real world. We have successfully deployed our policy in simulation and real-world experiments and tested the policy's performance in single-agent and multi-agent scenarios. Additionally, the policy can avoid intentional obstructions, like a rapid-moving obstacle controlled by a human.

Contribution. Our main contributions are as follows.

- We propose a multi-agent training platform based on a three-dimensional (3-D) simulator with a physical engine to bridge the gap between simulation and the real world. We compare a two-dimensional (2-D) simulator without a physics engine and a 3-D simulator with a physics engine with real-world environments. The result proves that a 3-D simulator with a physics engine can provide better randomness for agent training.
- We propose a lightweight end-to-end distributed multi-agent navigation policy, which utilizes the hidden state in the LSTM to alleviate the information loss in the POMDP. Besides, an attention structure based on the lightweight policy is proposed to improve the policy's performance in multi-agent scenarios. Both policies are trained in a stochastic environment and can be directly deployed to real-world robots.
- We propose a novel reward function to solve the problem: the agent may choose suboptimal actions in some common scenarios, such as passing through narrow gaps and multi-agent travels in the opposite direction.

The rest of this article is organized as follows. Section 2 is a brief review of the related work. Section 3 introduces the notation and formulation used in this article. Section 4 discusses the policy's structure, the RL setup for training multi-agent navigation policy, and the simulator platform. Section 5 presents the policy's performance in the simulator

and real-world experiments. Finally, we conclude our work and propose directions for future improvement in Section 6.

2 Related work

In this section, we briefly describe some related works of multi-agent navigation. These works can be categorized into trajectory-based, reaction-based, and learning-based approaches. The learning-based approaches can be further divided into supervised learning and RL. Finally, we discuss the approaches to bridge the gap between simulation and the real world.

2.1 Trajectory-based approaches

Trajectory-based approaches generally require detailed environmental information to plan a feasible trajectory for the robot (e.g., Model Predictive Control (MPC, [Keviczky et al. \(2004\)](#)) and Dynamic Window Approach (DWA, [Fox et al. \(1997\)](#))). In recent years, new theories, such as safe corridors, buffered Voronoi cells (BVC), and Graphs of Convex Sets (GCS), have been introduced to transform the navigation problem into a convex optimization problem. [Park et al. \(2023\)](#) utilizes a dynamic linear safe corridor while introducing mode-based subgoal planning to tackle planning problems in complex environments. They also use collision alert propagation and escape point planning to deal with emergencies. [Zhu et al. \(2022\)](#) constructs a chance-constrained buffered uncertainty-aware Voronoi cell (B-UAVC) for each robot and ensures the safety of robot navigation by specifying thresholds. [Marcucci et al. \(2023\)](#) proposes a framework that enables convex optimization to effectively and reliably plan trajectories around obstacles through a practical convex relaxation programming problem by using GCS. Although the trajectory-based algorithm can obtain the optimal trajectory, it will lead to large computational costs or difficult convex optimization when applied in large or unstructured scenarios.

2.2 Reaction-based approaches

Reaction-based approaches accomplish navigation tasks by continuously sensing and responding to the surrounding environment, enabling them to adapt to dynamically changing conditions. Reciprocal velocity obstacles (RVO) framework ([Fiorini and Shiller \(1998\)](#)) maps the dynamic environment into the robot velocity space and generates safe control velocities from these velocity constraints. The ORCA framework ([van den Berg et al. \(2011\)](#)) follows the principles of RVO while resolving the jitter problem in RVO and improves the obstacle avoidance efficiency. Moreover, [Alonso-Mora et al. \(2010\)](#) further guarantees smooth, collision-free motions under non-holonomic constraints. However, these approaches struggle to be implemented in the real world because they require a perfect perception of the agent's surroundings. In response to these limitations, some variants have been developed. [Godoy et al. \(2016\)](#) enhances environmental awareness through communication among agents, allowing for more accurate and timely adjustments based on shared information. [Arul and Manocha \(2021\)](#) incorporates Buffered Voronoi Cells to implement a more conservative obstacle avoidance policy, ensuring a safe

distance from obstacles and other agents. To some extent, these variants have solved the perception problem. Still, ORCA and its variants are sensitive to parameters, and the corresponding parameters are different in different scenarios, which makes these approaches difficult to adjust in practical applications.

2.3 Supervised learning-based approaches

With the advancement of machine learning, numerous studies utilize it to solve the robot navigation problem. Supervised learning-based approaches train the policy with extensive datasets, either through experts or traditional algorithms, and enable agents to learn how to map observations into actions. Yan et al. (2023) adopts an imitation learning approach, training a mapless navigation policy solely from 2-D LiDAR inputs, incorporating an aggregated dataset with additional safety enhancements. Karnan et al. (2022) utilizes imitation learning to devise a purely vision-based navigation algorithm, successfully learning navigation policies from a single video demonstration collected by physically distinct agents. Cho and Chung (2024) uses a risk-sensitive approach to prioritize learning on scarce but high-risk terrain through self-supervised learning and enriches reliable data for inexperienced terrain with pseudo-labels. Though supervised learning-based approaches have achieved significant breakthroughs in robot navigation, they struggle to cope with scenarios not represented in the training dataset. Furthermore, the reliance on expert knowledge inherently limits the policies from surpassing the boundaries of that preexisting knowledge.

2.4 Reinforcement learning-based approaches

RL can be applied well to navigation tasks since the robot navigation problem is a POMDP problem. RL-based multi-agent navigation approaches learn from the interaction, and the quality of the policy depends on the design of the reward function, the interaction quality, and the neural network's structure.

Generally, the reward function of the navigation problem is similar to the potential field function. Chen et al. (2017b) proposes a dense reward function that can guide reinforcement learning concisely and effectively. However, the reward function will cause the agent to learn suboptimal actions, which we will discuss in Section 4. Some approaches define the reward function through other rules. Chen et al. (2017a) develops a time-efficient navigation policy that respects public social norms by inducing the right-handed rules in the reward function. Xie and Dames (2023) introduces a velocity obstacle term into the reward function, enabling mobile robots to navigate autonomously in spaces filled with static obstacles and dense pedestrian traffic.

Some approaches train the policy in specific international scenarios. Li et al. (2019) proposes an advanced version of the Social Attention Reinforcement Learning (SARL) algorithm, achieving human-aware navigation in indoor environments. Yao et al. (2020) employs a grid map-based sensor fusion approach to map three frames of egocentric grid maps and the robot's relative local target positions into low-level robotic control commands. Huang et al. (2024)

provides the agent with a curriculum and a replay buffer of clipped collision segments, enhancing performance in obstacle-rich environments.

Regarding the neural network structure, some policies use CNNs to encode perceptual information, such as Liu et al. (2020), Guldenring et al. (2020), Chen et al. (2021). To enhance the policy's utilization of past states, some approaches harness the hidden state structure of RNNs to store historical information. Liu et al. (2021) presents the Decentralized Structured Recurrent Neural Network (DS-RNN), which uses spatial and temporal relationships for robotic decision-making in swarm navigation. Xue and Chen (2024) introduces a novel multi-agent recurrent deterministic policy gradient algorithm and leverages LSTM to improve action value predictions using historical exploration information.

Some traditional control approaches have also been employed to enhance the safety of RL training. Cheng et al. (2019) utilizes a model-based controller leveraging Control Barrier Functions (CBFs) and online learning of unknown system dynamics to ensure safety during the learning phase. Emam et al. (2022) incorporates safety as a differentiable robust control barrier function layer within a model-based RL framework and proposes a modular approach to learning potential reward-driven tasks independently of safety constraints.

2.5 Simulation-to-real gap

As training is inefficient in the real world and easily damages the robot, RL-based approaches are usually trained in simulators. Kahn et al. (2021) proposed an approach to collect data in reality and train policy that can navigate in real-world urban and off-road environments with geometrically distracting obstacles. However, the gap between simulations and real-world environments remains a crucial barrier preventing the widespread adoption of RL-based approaches in real robots. Several approaches have been proposed to address this issue and bridge the simulation-to-reality gap. Rusu et al. (2016) utilizes progressive networks to bridge the reality gap and transfer policies learned in simulation to the real world. Tobin et al. (2017) investigates domain randomization, a straightforward technique for training models on simulated images that transfers to real images by randomizing renderings within the simulator. García and Molina (2019) proposes an approach to evaluate LiDAR sensors and navigation and obstacle avoidance capabilities in simulated scenarios using a real drone platform. Fan et al. (2020) proposes a hybrid control RL approach, which initially learns an end-to-end general obstacle avoidance policy through RL. Subsequently, hybrid control is incorporated into this policy to improve its feasibility and robustness in real-world environments. This approach leverages the strengths of both RL for learning complex behaviors and hybrid control to ensure reliability and stability in practical applications. Shi et al. (2023) proposed a domain adaptation approach based on a cyclic consistent generative adversarial network and a force control transfer approach to bridge the reality gap.

Our approach further bridges the gap between simulation and the real-world environment by designing a training platform based on a physics-based simulator. We also

propose a novel policy network based on LSTM and attention mechanism, which is state of the art (SOTA) of the navigation based on pure LiDAR sensor. Furthermore, a novel reward function is designed to solve some common scenarios, such as agent passes through narrow gaps.

3 Problem formulation

In this section, we will introduce the notation of this work and our reward function.

3.1 Notation of reinforcement learning

This work models the multi-agent navigation process as POMDP. The POMDP can be defined as $\langle \mathcal{I}, \mathcal{S}, \mathcal{O}, \mathcal{A}, \mathcal{R}, \mathcal{T}, done, \gamma \rangle$, where $\mathcal{I} = \{1, \dots, N\}$ denotes N agents, \mathcal{S} denotes the set of states of all agents, $\mathcal{O} = \{\mathcal{O}_1, \dots, \mathcal{O}_N\}$ denotes the set of observable state of agents, \mathcal{A} denotes the set of actions, \mathcal{R} denotes the reward function, $\mathcal{T} : \mathcal{S} \times \mathcal{A} \mapsto \mathcal{S}$ denotes the transfer function and $done$ indicates whether an episode has terminated in time or collided with an obstacle, and $\gamma \in [0, 1)$ denotes the discount factor. At each time step t , the agent's observation is $o^t = [o_s^t, o_g^t, o_v^t]$, where $o_s^t \in \mathbb{R}^{5 \times L_n}$ is formed by concatenating 5 consecutive frames of LiDAR data, with L_n being the measurement dimension of the LiDAR data; $o_g^t \in \mathbb{R}^2$ consists of the distance from the agent's current position to the goal point, and the angle between the agent's orientation and the direction towards the goal point; $o_v^t = [v_i^t, \omega_i^t] \in \mathbb{R}^2$ consists of the agent's linear and angular velocities. The agent i receives o_i^t and executes action a_i^t according to policy $\pi_\theta(a_i^t | o_i^t)$, where θ is the policy parameter. The policy $\pi_\theta(a_i^t | o_i^t)$ is a Gaussian distribution, with the mean calculated by a policy network. The action $a_i^t = [v_i^t, \omega_i^t]$ is sampled from the policy $\pi_\theta(a_i^t | s_i^t)$. The state s_t takes the action set a_1^t, \dots, a_N^t to transfer to next state s_{t+1} according to $\mathcal{T}(s_{t+1} | s_t, a_1^t, \dots, a_N^t)$. Also, the next observable state set is updated as $\mathcal{O} = \mathcal{T}(\{\mathcal{O}_1, \dots, \mathcal{O}_N\} | s_t, a_1^t, \dots, a_N^t)$, and the reward set is obtained by $\mathcal{R} = \{r(s_1^t, a_1^t), \dots, r(s_N^t, a_N^t)\}$. A trajectory can be represented as $\langle o^1, a^1, r^1, o^2, a^2, r^2, \dots, s^T, a^T, r^T \rangle$, where T represents the number of interaction steps. Each agent i aims to maximize the discounted future reward: $G_i^t = \sum_{t=0}^T \gamma^t r_i^t$. The state-value function is defined as $V^\pi(s) = \mathbb{E}[\sum_{t=0}^T \gamma^t R^t | s^1 = s]$, and the action-value function is given by $Q^\pi(s, a) = \mathbb{E}[R(s, a) + \gamma V^\pi(s) | s^1 = s, a^1 = a]$. A action is chosen as $a = \arg \max_a Q(s, a)$.

3.2 Reward function

The dense reward function used in RL-based navigation algorithms consists of distance reward, obstacle penalty, and efficiency reward. An example of such a reward function is:

$$\begin{aligned} R &= r_g + r_c + r_{other}, \\ r_g &= \begin{cases} r_{arrival} & \text{if } \|p_i^t - g_i\| < 0.1, \\ w_g (\|p_i^{t-1} - g_i\| - \|p_i^t - g_i\|) & \text{otherwise,} \end{cases} \\ r_c &= \begin{cases} r_{collision} & \text{if } d_i^t < 0, \\ w_c (0.1 - d_i^t/2) & \text{if } d_i^t < 0.2, \\ 0 & \text{otherwise,} \end{cases} \end{aligned} \quad (1)$$

where r_{other} is the other reward that varies in different approaches, r_g means the distance reward, which is computed as the difference in the distance between the robot and the goal point at the current time step and the previous time step, r_c means the obstacle penalty, w_g and w_c are the weight of r_g and r_c respectively, d_i^t means the smallest distance between agent i and obstacles at time step t . However, this reward function setup may make agents learn conservative policy. Additionally, many works impose control constraints, such as velocity and angular velocity, on r_{other} to maintain action coherence. Too many constraints may lead to instability in the training process and difficulty adjusting the weights between various terms. Moreover, in some scenarios, the reward function does not adequately indicate optimal actions.

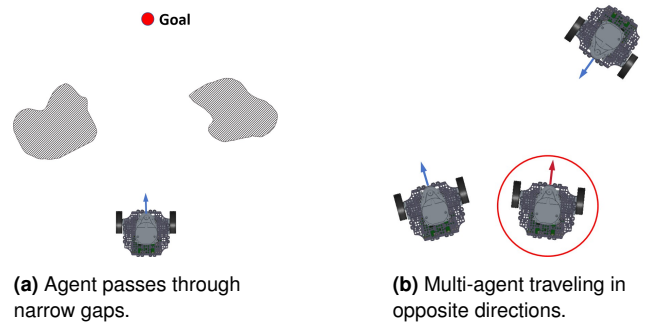


Figure 1. Cases that are difficult to handle with the classical reward function.

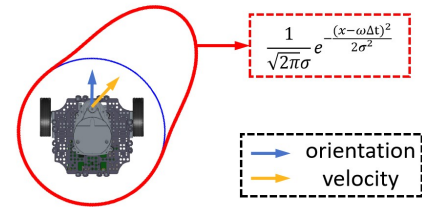


Figure 2. The weight of the scan penalty of the r'_c .

As shown in Figure 1, when an agent needs to navigate through the gap between two obstacles, it may incur penalties due to r_c when approaching them, even though traversing the gap is the optimal action. Consequently, the agent may choose to circumnavigate around the obstacles instead. Besides, when multiple agents approach each other, they may only focus on the closest agent or obstacle to itself, neglecting potentially threatening agents that are further away but pose a real danger, which leads to unsafe navigation. To address the issues above, we have introduced modifications to the r_c component, specifically by:

$$r'_c = \begin{cases} r_{collision} & \text{if } d_i^t < 0, \\ w'_c (l - sl_i^t) + r_c & \text{otherwise,} \end{cases} \quad (2)$$

where $r_{arrival} = 5$, $r_{collision} = -5$, $w_g = 5$, $w'_c = -0.25$, $w_c = -0.03$, l represents the maximum length of the LiDAR rays, sl_i^t represents the LiDAR information of agent i at time step t , w'_c is a weight vector that varies with angular velocity,

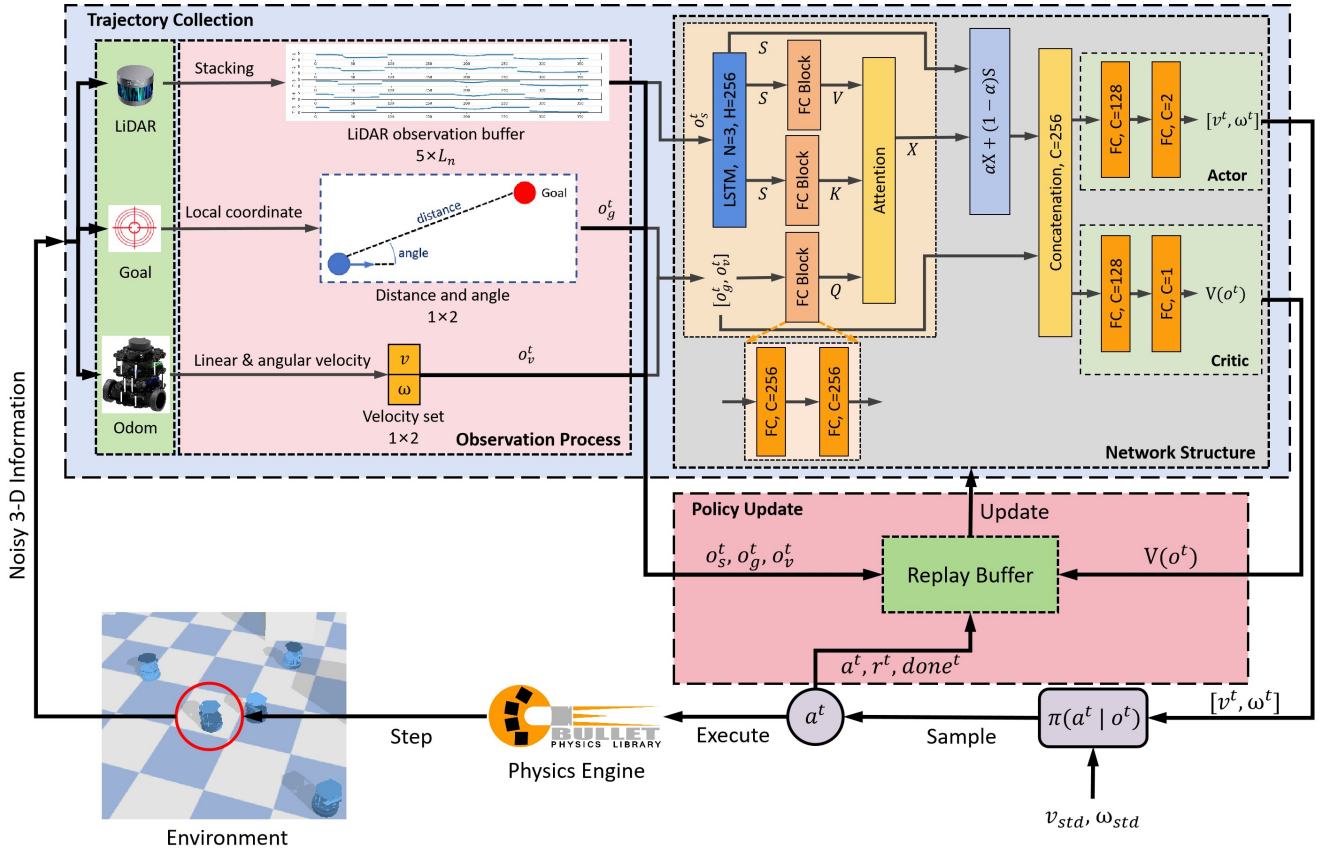


Figure 3. The overall framework diagram of our approaches is presented. The approaches can be divided into trajectory collection and policy update. During trajectory collection, each agent collects the trajectory independently and stores it in a replay buffer. The simulation platform will return each agent's reward and observation after an action is executed. After a specific number of iterations, the trajectories stored in the replay buffer will be used to calculate the loss, and the network will then be updated based on the loss through gradient descent. The two stages alternate until a specific number of episodes is reached or the policy converges.

with the weight decreasing in $\frac{1}{\sqrt{2\pi}\sigma} e^{-\frac{(x-\omega\Delta t)^2}{2\sigma^2}}$ fashion from $\omega\Delta t$ towards both sides, where $\sigma = 0.2$, Δt is the time interval. The schematic diagram of w'_c is shown in Figure 2.

Using r'_c , the policy pays more attention to the direction of the current angular velocity while maintaining the closest distance to the surrounding obstacles. This allows the policy to better cope with the mentioned situations and allows the agent to pay more attention to the choice of angular velocity.

4 Method

In this section, we will introduce the architecture of the policy network, the simulation platform, and the training process with training scenarios. We utilize the hidden state of LSTM to compensate for the lack of information in the observations and propose an attention structure to improve the policy ability in the multi-agent scenario. Besides, we propose a multi-agent simulation platform to bridge the gap between simulation and the real world. Additionally, the multi-agent training process is based on Proximal Policy Optimization (PPO, Schulman et al. (2017)), with modifications in trajectory collection. Finally, we use two scenarios for training: single-agent and multi-agent.

4.1 Network structure

We note that the agent only requires more biased actions toward the goal point when approaching it. In other situations, the agent merely needs to move in a general direction. As such, we clip the distance between the agent and the goal point to enable the policy to better distinguish between these two situations rather than directly using the distance as an input to the network.

We first only use LSTM to encode the LiDAR observation. The policy is trained in a static environment and works well in static and 6-agent test environments. However, it performs poorly when the robot's number increases over 6. Thus, we add an attention module to overcome the issue. As shown in Figure 3, we use a three-layer LSTM module to encode the laser measurements o_s^t , with both hidden sizes = 256, and get S . Then, K and V are calculated by two different FC layers by using S , in which the output sizes = 256. At the same time, $[o_g^t, o_v^t]$ passes through two FC layers, which output sizes = 256, to obtain Q . Then, the encoding of o_s^t , X , is obtained by multi-head attention:

$$\begin{aligned} \text{MultiHead}(Q, K, V) &= \text{Concat}(\text{head}_1, \dots, \text{head}_h)W^O, \\ \text{where } \text{head}_i &= \text{Attention}(QW_i^Q, KW_i^K, VW_i^V), \\ \text{Attention}(Q, K, V) &= \text{Softmax}\left(\frac{QK^T}{\sqrt{d_k}}\right)V, \end{aligned} \quad (3)$$

where d_k is the size of K . The final encoding is obtained by the weighted sum of X and S with an adaptive residual

Algorithm 1 PPO For Multi-Agent training

```

1: procedure PPO(environment, hyperparameters)
2:   Initialize policy network  $\pi_\theta$ , value function network  $V_\phi$ , and set hyper-parameters
3:   for  $iteration = 1, 2, \dots$ , do
4:     for  $t = 1, 2, \dots, T_{max}$  do
5:       for robot  $i = 1, 2, \dots$  do
6:         Run policy network  $\pi_\theta$ , collecting  $\{o_i^t, a_i^t, r_i^t\}$ .
7:         Run value function network, collecting  $\{V_\phi(o_i^t)\}$ 
8:       end for
9:     end for
10:    for robot  $i = 1, 2, \dots$  do
11:      for  $t = T_{max}, T_{max}-1, \dots, 1$  do
12:        Calculate TD-error:  $\delta_i^t = r_i^t + \gamma V_\phi(o_i^{t+1}) - V_\phi(o_i^t)$ 
13:        Estimate advantages using GAE:  $A_i^t = \sum_{t'=t}^{T_{max}} (\gamma\lambda)^{t'-t} \delta_i^{t'}$ 
14:        Calculate  $V_i^t = A_i^t + V_\phi(o_i^t)$ 
15:      end for
16:    end for
17:    Merge and shuffle the collected trajectories
18:     $\theta_{old} = \theta, \phi_{old} = \phi$ 
19:    for epoch in Epoch do
20:       $L^{PPO} = -\mathbb{E} \left( \sum_{i=1}^N \sum_{t=1}^{T_{max}} \min \left( \frac{\pi_\theta(a_i^t|o_i^t)}{\pi_{\theta_{old}}(a_i^t|o_i^t)} A_i^t, \text{clip} \left( \frac{\pi_\theta(a_i^t|o_i^t)}{\pi_{\theta_{old}}(a_i^t|o_i^t)}, 1 - \epsilon, 1 + \epsilon \right) A_i^t \right) \right)$ 
21:       $L^V = \max \left( \mathbb{E} \left( \sum_{i=1}^N \sum_{t=1}^{T_{max}} \left( (V_\phi(o_i^t) - V_i^t)^2, (\text{clip}(V_\phi(o_i^t), V_{\phi_{old}}(o_i^t) - \epsilon, V_{\phi_{old}}(o_i^t) + \epsilon) - V_i^t)^2 \right) \right) \right)$ 
22:       $L^{Entropy} = H(\pi_\theta(a^t|o^t))$ 
23:       $L^{Total} = L^{PPO} + \alpha L^V + \beta L^{Entropy}$ 
24:      Update the parameters of  $\pi_\theta$  and  $V_\phi$  using Adam Optimizer w.r.t  $L^{Total}$ 
25:    end for
26:  end for
27: end procedure

```

adjustment, $\alpha X + (1 - \alpha)S$, where α updates with the policy and the value network. In actor and critic, the final encoding is decoded by two fully connected layer (FC) layers with output size = 128 and output size = 2 to get the mean of the policy $[v^t, \omega^t]$, and another two FC layers with output size = 128 and output size = 1 to get the value network $V_\phi(o^t)$. Note that each LSTM layer is followed by a rectified linear unit (ReLU), and so is the FC layer. Additionally, the last FC layer of the actor and critic modules has no ReLU layers.

4.2 Simulation platform

To bridge the gap between simulation and the real world, we propose a multi-agent training platform based on a physics-based simulator such as Pybullet (Coumans and Bai (2016–2021)) and Gazebo. In most 2-D simulators, the actions of the agent are usually perfectly executed, and their positions are usually calculated by $x^{t+1} = x^t + v^t \Delta t + \frac{1}{2} a^t \Delta t^2$. In a physics-based simulator, the agent state is computed by the physics engine, i.e., $x^{t+1} = T(x^t, v^t, a^t, f^t, \dots)$, where T is the transfer function of the physics engine, f^t is the force acting on the agent. The transfer function T makes the execution of the action randomness. A straightforward example is when the straight action executes in different types of simulators, the results differ. As shown in Figure 4. The 2-D simulator executes the action without bias, while the agent in the physics-based simulator deviates from the straight line, and the deviation is greater in real-world robots. This indicates that training on a physics-based simulator

may help the agent learn more realistic policies, thereby facilitating the deployment of the policy on actual robots. To better train the policy, we add Gaussian noise to the agent's perception to increase randomness further.

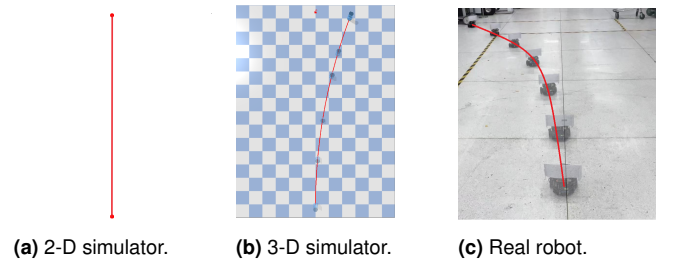


Figure 4. Comparison between the simulators and the real world. Agents on all platforms execute commands with $v = 1 \text{ m/s}$, $\omega = 0 \text{ rad/s}$. The direct travel distance of the agent in the simulator is 10m, and the distance of the real robot is 5 m.

We propose a local replay mechanism for the trajectory collection of the agent's collision aiming to speed up the collection of multi-agent interaction trajectories. When the agent collides, the agent will be reset back to the state before the N simulation steps so that the agent can quickly accumulate the collision data and speed up the training, where $N = 300$ in this article. However, when the local replay mechanism is deployed in a multi-agent scenario, the reset agent may appear in front of the normal agent, causing the normal agent to be disturbed. Sudden disturbances may make the policy conservative. However, we found that in

some cases, agents perform slowing or stopping actions to wait for other agents to leave.

Besides, to make the simulator generalize, we adopt the architecture of Gym (Brockman et al. (2016)), and we have diligently maintained the interfaces intending to provide users with a more convenient experience when utilizing the simulator. The simulator supports the random addition of random or queued agents or obstacles and controls the movement of each agent through a action set \mathcal{A} . At the end of a simulator step, the simulator returns a observed state set \mathcal{O} . The update frequency of the simulator can be modified to meet the policy training at different control frequencies. All of these functionalities are designed for easy reconfiguration. For example, to accommodate users seeking to evaluate Safe Reinforcement Learning (Safe-RL, Achiam and Amodei (2019)), we have reconfigured our custom-designed simulator to include a constrained version by changing two functions of the origin version.

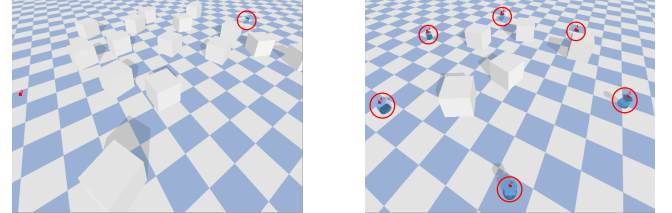
4.3 Training process

We treat distributed multi-agent navigation as plenty of single agents navigating in an unknown environment, meaning each agent collects the trajectory respectively. As shown in Figure 3, the training process can be divided into trajectory collection and policy update. During the trajectory collection, each agent first observes the LiDAR o_s^t , target point o_g^t , and velocity o_v^t . After that, it utilizes the policy and value network to calculate a value v^t and an action mean $[v^t, \omega^t]$. From these, an action a^t is sampled based on the policy distribution $\pi_\theta(a^t|o^t)$ and executed. The simulator then responds with a reward r^t , the next state o^{t+1} , and a termination signal $done^t$. The tuple of $\langle o^t, a^t, r^t, o^{t+1}, done^t, V_\phi(o^t) \rangle$ is stored in replay buffer. This process is repeated until a specified number of iterations have been completed. Subsequently, the trajectories stored in the relay buffer are used to calculate the total loss L^{Total} for updating the policy and value networks. After updating the networks, the replay buffer will be cleared, and the agents collect trajectories again. The two stages alternate until convergence or episode limit is reached.

Alg 1 shows a more detailed training process. In lines 3-9, each agent collects the trajectories respectively and calculates the values using the value network under the same environment. After specific steps, in lines 10-15, according to the trajectories collected by each agent, the corresponding advantages of each trajectory are calculated through General Advantage Estimation (GAE, Schulman et al. (2015)). Then, we merge and shuffle the trajectories to get training data. In lines 17-24, we calculate the policy loss by $L^{PPO} = \min(\frac{\pi_\theta(a|s)}{\pi_{\theta_{old}}(a|s)} A, \text{clip}(\frac{\pi_\theta(a|s)}{\pi_{\theta_{old}}(a|s)}, 1 - \epsilon, 1 + \epsilon) A)$, the value loss by $L^V = \max((V_\theta - V_{target})^2, (\text{clip}(V_\theta, V_{\theta_{old}} - \epsilon, V_{\theta_{old}} + \epsilon) - V_{target})^2)$, where $V_{target} = A + V_\phi(s)$ and the entropy loss by $L^{Entropy} = H(\pi_\theta(a^t|o^t))$. We get the total loss by weighted summing $L^{Total} = -L^{PPO} + \alpha L^V + \beta L^{Entropy}$, where α and β are hyperparameters. We use the Adam Optimizer (Kingma and Ba (2014)) to update the policy and value network w.r.t L^{Total} . The algorithm proceeds to the next iteration until a specified iteration is reached. We also use some tricks to make the training more stable. The tricks include reward

scaling (Gao et al. (2022)), mini-batch updating, advantage normalizing, and learning rate decay.

We use two scenarios during training: single-agent and multi-agent. As we clip the distance input to the network, the size of the scenario does not affect the training. Thus, in the single-agent scenario, the initial point and the goal point of navigation are 10 m apart and the multi-agent scenario's initial and goal navigation points are 16 m apart. The two scenarios are shown in Figure 5.



(a) Single-agent scenario.

(b) Multi-agent scenario.

Figure 5. The two scenarios during training, where the robot is circled by a red box. In a single-agent scenario, 15 obstacles are randomly placed in an area of 5 m \times 5 m. In multi agents scenario, 6 agents are placed in a circle queue, and 5 obstacles are randomly placed in an area of 5 m \times 5 m.

The environment for each scenario is generated in real-time during training, and the agents do not have any prior knowledge of the environment. The environment contains randomly placed obstacles, an obstacle refers to a 1 m \times 1 m \times 1 m cube, and a random placed obstacle means that its position and orientation are random, which makes the environment unstructured. The random obstacles are positioned within a range of 5 m \times 5 m, with no limitations on their orientation. When training in the single-agent scenario, we first place 5 random obstacles and then increase to 15 random obstacles. The scenario with 5 random obstacles is used to verify the feasibility of the policy, and the scenario with 15 random obstacles is used to train the policy of navigating in a static and messy environment. We then retrain the policy of the single-agent scenario in the multi-agent scenario. The multi-agent scenario consists of 6 agents placed in a circle queue and 5 random obstacles.

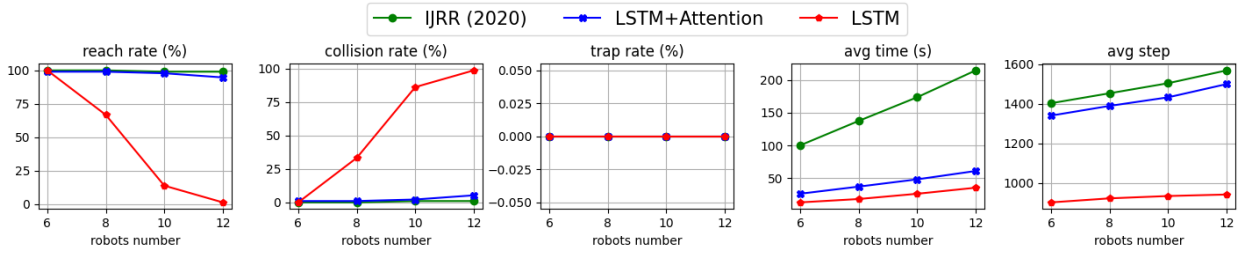
The measurement dimension L_n of the LiDAR of the policy is different, and the max length of the LiDAR beam is 4 m. We first train the policy with $L_n = 36$, which works successfully in the single-agent scenario. In the multi-agent scenario, the L_n of LSTM policy and LSTM+Attention are 72. Because, if $L_n = 36$, the agent may lose information when other agents stay in the internal of the LiDAR beam, with the biggest internal = 0.34 m, while $L_n = 72$, the biggest internal = 0.17 m is enough for most situations. The field of view (FOV) is set to π rad. Additionally, we stack the LiDAR observations of 5 consecutive frames to provide more comprehensive observation information. The agent's velocity is set within the $[0, 1]$ m/s, and the angular velocity is set within the $[-\pi, \pi]$ rad/s. The control frequency used in training is 60 Hz, which can make the reward variation of each action more apparent and maintain efficient control. Finally, the maximum number of simulation steps is set to 2500, sufficient for the agent to finish navigation through the optimal path.

Table 1. Experiment with 1 robot and 15 obstacles.

	success rate(%)	collision rate(%)	trap rate (%)	average step
IJRR (Fan et al. (2020))	91.3	8.6	0.1	1383.23
Linear policy	67.2	2.4	30.4	550.40
LSTM policy	93.1	6.9	0.0	1187.73
LSTM+Attention	95.9	3.9	0.2	1300.78
(Safe) LSTM+Attention	97.6	2	0.04	1353.63

Table 2. Experiment with 6 robots and 5 obstacles.

	success rate(%)	collision rate(%)	trap rate (%)	average step
NH-ORCA (Alonso-Mora et al. (2010))	98.4	0.33	1.27	1198.82
IJRR (Fan et al. (2020))	85.03	14.63	0.33	1617.84
LSTM policy	91.89	8.15	0.0	981.01
LSTM+Attention	94.78	4.68	0.53	1805.94

**Figure 6.** Multi-agent test without obstacle.

5 Experiments

To evaluate the ability of the policy, we test it in both simulation and the real world compared with NH-ORCA (Alonso-Mora et al. (2010)) and the policy of Fan et al. (2020). In the following section, we refer to the policy of Fan et al. (2020) by CNN-policy, and the measurement dimension of the LiDAR $L_n = 512$. The LSTM+Attention policy is the proposed policy. We conducted an ablation experiment by removing the attention mechanism from the proposed policy, which is LSTM policy. Additionally, we replaced the LSTM layer with a Linear layer and get the Linear policy, in order to validate the effectiveness of the LSTM layer. In the simulation tests, we use some metrics to evaluate the policy. The metrics consist of the success rate, the collision rate, the trap rate, and the average step. The success rate means the agent's success rate navigates to the goal in time without collision. The collision rate means the rate at which the agent collides with other objects. The trap rate means the rate at which agent cannot reach the goal in time and without collision. The average step is the average simulation step of the agent to reach the goal successfully. We use the simulation step rather than the cost time of navigation because the cost time depends on the calculation speed of the simulator, which cannot exactly reflect the cost time of navigation. Finally, all simulation tests are performed 1000 times.

5.1 Simulation test

The single-agent test environment is set up as 1 robot, 15 obstacles (5 m × 5 m). The result is shown in Table 1. As a result, the LSTM+Attention policy performs better where the success and collision rates are 4.6% higher and 4.7% lower than the CNN policy. The trap rate is 0.1% higher than the

CNN policy because the LSTM+Attention policy will rotate around the target point after approaching the goal point. The angular velocity of the differential wheel robot will make the robot rotate around the center $r_c = \frac{(v_l + v_r)d_{wb}}{2(v_r - v_l)}$ of its central point when it has nonzero linear velocity, where v_l is the left wheel rotate velocity, v_r is the right wheel rotate velocity, d_{wb} is the wheel distance. However, the LSTM policy doesn't have such a problem, as the trap rate is 0% and is the fastest policy. We also train our method within Safe-RL and get the best test result in the success rate and collision rate.

The environment of the multi-agent test is set up as 6 robots and 5 obstacles (5 m × 5 m). The result is shown in Table 2. The reach rate of the LSTM policy and the LSTM+Attention policy is 6.86% and 9.75% higher than the CNN policy. Also, the collision and trap rates of the LSTM policy are 6.48% and 0.33% better than the CNN policy, while the LSTM+Attention are 9.95% lower and 0.2% higher than CNN policy, respectively. Besides, the LSTM costs minimal simulation step again. Compared with NH-ORCA, which has all precise environment and agent information, our algorithm also has a certain competitiveness in trap rate and average step, in which the LSTM policy is 1.27% lower and 217.81 steps faster than NH-ORCA. To avoid losing generality, we also do some tests without obstacles; the result is shown in Figure 6. The CNN policy performs best and does not decrease significantly as the agents' number increases. Besides, the LSTM+Attention policy is slightly worse than CNN policy, with a slight decline in numbers as the number increases. Finally, the LSTM policy proves to be the least effective, as it fails to complete navigation when the number of agents surpasses 6.

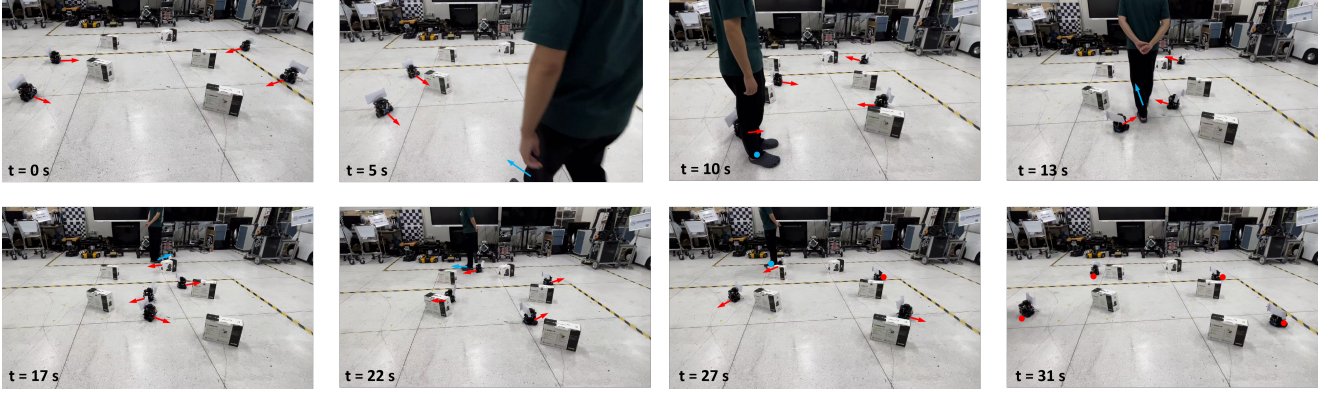


Figure 7. Real-world multi-agent experiment. The red pattern indicates the state of turtlebot3, the blue pattern indicates the state of a human, the arrow represents the direction of velocity, and the circle represents reaching the goal point (turtlebot3) or remaining stationary (human). At $t = 0$ s, each turtlebot3 navigates to the goal point. A human appears in the environment at $t = 5$ s, starting to interfere with turtlebot3. The human first forces a turtlebot3 to change its trajectory and crosses in front of two turtlebot3s at $t = 10$ s and $t = 13$ s. Then, the human interferes with another turtlebot3 again until it reaches the goal point for the rest of the time. All turtlebot3s reach the goal points in 31 s.

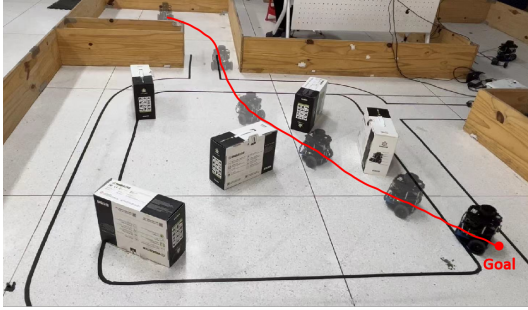


Figure 8. Real-world single-agent experiment. The turtlebot3 first passes through narrow passages, then crosses through the obstacles, and finally reaches the goal point. The turtlebot3 reaches the goal point in 46 s.

5.2 Real-world test

We use turtlebot3 to test the policy’s performance in the real world. As the max linear velocity and angular velocity of the turtlebot3 are 0.2 m/s and 1 rad/s, we scale the output of our policy to fit the ability of turtlebot3. Besides, the control frequency of turtlebot3 is set to 10 Hz. The observation of the LiDAR given by turtlebot3 with parameters are $FOV = 2\pi$ rad, and LiDAR beam number = 360. We only use 72 LiDAR beam with $FOV = 0.8\pi$ rad. We align the rest of the policy with the simulation settings. We use the wheel odometry and LiDAR sensor on the turtlebot3 for perception. Wheel odometry calculates the robot’s relative position and angle to the goal point, while the LiDAR sensor is employed to gather LiDAR observation. Although it is possible to let each turtlebot3 calculate its action independently, it is unable to install the corresponding library, like Pytorch [Paszke et al. \(2017\)](#), on the onboard Raspberry Pi. Therefore, we control turtlebot3 through the Robot Operating System (ROS, [Quigley et al. \(2009\)](#)) communication protocol by using a host computer.

In the single-agent scenario, we test the performance of the policy through narrow passages. The turtlebot3 passes and avoids obstacles with unknown positions and shapes to reach the goal point. As shown in Figure 8, the turtlebot3 starts at a room and passes through a passage to get in the room

with the goal point in 22 s. Then, the turtlebot3 crosses the obstacles to reach the goal point in 24 s. At last, the turtlebot3 finishes the navigation when approaching the goal point.

In the multi-agent scenario, we test the policy’s performance in avoiding other agents and sudden disturbances. A turtlebot3 needs to go through obstacles and avoid other turtlebot3. Besides, a human who wants to interfere with turtlebot3 is a sudden disturbance. As shown in Figure 7, at first, the human appears in front of a turtlebot3 to force it to change its trajectory, and after that, the human directly crosses through two turtlebot3. Then, the human continues to interfere with other turtlebot3 until it reaches its goal point. All turtlebot3s successfully avoid collision with other turtlebot3s and the human.

These two experiments prove that the policies trained on our proposed simulation platform can be directly deployed on real robots, with only adjustments made to the values of output actions based on the real robot’s capabilities.

6 Conclusion

This paper proposes a lightweight, end-to-end multi-agent navigation policy that translates raw LiDAR observation directly into action commands, eliminating the need to distinguish between dynamic and static obstacles and enabling navigation through narrow gaps. A physics-engine-based simulation platform is introduced for multi-agent training, bridging the gap between simulation and reality. Our method, trained using RL, demonstrates robust performance in simulated and real-world environments, even in malicious obstructions.

Key contributions include the proposal of a distributed navigation policy trained in stochastic environments, the utilization of LSTM to mitigate information loss in POMDP, the development of a multi-agent training platform to facilitate idea validation and safe RL, and the introduction of a new reward function to address suboptimal action selection. The policy’s performance is evaluated in simulation and real-world settings, highlighting its effectiveness and potential for future enhancements.

In the future, we will explore extending the policy to more complex environments, incorporating passing through traffic, or expanding the work to Unmanned aerial vehicles (UAVs). We will further refine the reward function and the policy to enhance performance in edge cases, like U-shaped obstacles.

Acknowledgements

This work is supported by Shenzhen Science and Technology Program under Grant RCBS20221008093305007, Grant 20231115141459001, Young Elite Scientists Sponsorship Program by CAST under Grant 2023QNRC001, and High level of special funds (G03034K003) from Southern University of Science and Technology, Shenzhen, China.

References

- Achiam J and Amodei D (2019) Benchmarking safe exploration in deep reinforcement learning. URL <https://api.semanticscholar.org/CorpusID:208283920>.
- Alonso-Mora J, Breitenmoser A, Ruffi M, Beardsley PA and Siegwart RY (2010) Optimal reciprocal collision avoidance for multiple non-holonomic robots. In: *International Symposium on Distributed Autonomous Robotic Systems*. URL <https://api.semanticscholar.org/CorpusID:17699054>.
- Arul SH and Manocha D (2021) V-rvo: Decentralized multi-agent collision avoidance using voronoi diagrams and reciprocal velocity obstacles. In: *2021 IEEE/RSJ International Conference on Intelligent Robots and Systems (IROS)*. pp. 8097–8104. DOI:10.1109/IROS51168.2021.9636618.
- Brockman G, Cheung V, Pettersson L, Schneider J, Schulman J, Tang J and Zaremba W (2016) Openai gym.
- Chen G, Pan L, Chen Y, Xu P, Wang Z, Wu P, Ji J and Chen X (2020) Robot navigation with map-based deep reinforcement learning. In: *2020 IEEE International Conference on Networking, Sensing and Control (ICNSC)*. pp. 1–6. DOI:10.1109/ICNSC48988.2020.9238090.
- Chen L, Zhao Y, Zhao H and Zheng B (2021) Non-communication decentralized multi-robot collision avoidance in grid map workspace with double deep q-network. *Sensors (Basel, Switzerland)* 21. URL <https://api.semanticscholar.org/CorpusID:231761670>.
- Chen YF, Everett M, Liu M and How JP (2017a) Socially aware motion planning with deep reinforcement learning. In: *2017 IEEE/RSJ International Conference on Intelligent Robots and Systems (IROS)*. pp. 1343–1350. DOI:10.1109/IROS.2017.8202312.
- Chen YF, Liu M, Everett M and How JP (2017b) Decentralized non-communicating multiagent collision avoidance with deep reinforcement learning. In: *2017 IEEE International Conference on Robotics and Automation (ICRA)*. pp. 285–292. DOI:10.1109/ICRA.2017.7989037.
- Cheng R, Orosz G, Murray RM and Burdick JW (2019) End-to-end safe reinforcement learning through barrier functions for safety-critical continuous control tasks. In: *AAAI Conference on Artificial Intelligence*. URL <https://api.semanticscholar.org/CorpusID:58097250>.
- Cho I and Chung W (2024) Learning self-supervised traversability with navigation experiences of mobile robots: A risk-aware self-training approach. *IEEE Robotics and Automation Letters* 9(5): 4122–4129. DOI:10.1109/LRA.2024.3376148.
- Coumans E and Bai Y (2016–2021) Pybullet, a python module for physics simulation for games, robotics and machine learning. <http://pybullet.org>.
- Cui Y, Lin L, Huang X, Zhang D, Wang Y, Jing W, Chen J, Xiong R and Wang Y (2022) Learning observation-based certifiable safe policy for decentralized multi-robot navigation. In: *2022 International Conference on Robotics and Automation (ICRA)*. pp. 5518–5524. DOI:10.1109/ICRA46639.2022.9811950.
- Dutta A, Roy S, Kreidl OP and Bölöni L (2021) Multi-robot information gathering for precision agriculture: Current state, scope, and challenges. *IEEE Access* 9: 161416–161430. DOI:10.1109/ACCESS.2021.3130900.
- Emam Y, Notomista G, Glotfelter P, Kira Z and Egerstedt M (2022) Safe reinforcement learning using robust control barrier functions. *IEEE Robotics and Automation Letters* : 1–8 DOI:10.1109/LRA.2022.3216996.
- Fan T, Long P, Liu W and Pan J (2020) Distributed multi-robot collision avoidance via deep reinforcement learning for navigation in complex scenarios. *The International Journal of Robotics Research* .
- Fiorini P and Shiller Z (1998) Motion planning in dynamic environments using velocity obstacles. *The International Journal of Robotics Research* 17(7): 760–772. DOI:10.1177/027836499801700706. URL <https://doi.org/10.1177/027836499801700706>.
- Fox D, Burgard W and Thrun S (1997) The dynamic window approach to collision avoidance. *IEEE Robotics and Automation Magazine* 4(1): 23–33. DOI:10.1109/100.580977.
- Gao L, Schulman J and Hilton J (2022) Scaling laws for reward model overoptimization. In: *International Conference on Machine Learning*. URL <https://api.semanticscholar.org/CorpusID:252992904>.
- García J and Molina JM (2019) Simulation in real conditions of navigation and obstacle avoidance with px4/gazebo platform. In: *2019 IEEE International Conference on Pervasive Computing and Communications Workshops (PerCom Workshops)*. pp. 979–984. DOI:10.1109/PERCOMW.2019.8730764.
- Godoy J, Karamouzas I, Guy SJ and Gini ML (2016) Implicit coordination in crowded multi-agent navigation. In: *AAAI Conference on Artificial Intelligence*. URL <https://api.semanticscholar.org/CorpusID:6562091>.
- Guldenring R, Görner M, Hendrich N, Jacobsen NJ and Zhang J (2020) Learning local planners for human-aware navigation in indoor environments. In: *2020 IEEE/RSJ International Conference on Intelligent Robots and Systems (IROS)*. pp. 6053–6060. DOI:10.1109/IROS45743.2020.9341783.
- Han R, Chen S, Wang S, Zhang Z, Gao R, Hao Q and Pan J (2022) Reinforcement learned distributed multi-robot navigation with reciprocal velocity obstacle shaped rewards. *IEEE Robotics and Automation Letters* 7(3): 5896–5903. DOI:10.1109/LRA.2022.3161699.
- Hochreiter S and Schmidhuber J (1997) Long short-term memory. *Neural Computation* 9: 1735–1780. URL <https://api.semanticscholar.org/CorpusID:1915014>.
- Huang Z, Yang Z, Krupani R, Şenbaşlar B, Batra S and Sukhatme GS (2024) Collision avoidance and navigation for a quadrotor swarm using end-to-end deep reinforcement learning. In: *2024 IEEE International Conference on Robotics and Automation (ICRA)*. pp. 300–306. DOI:10.1109/ICRA57147.2024.10611499.

- Kahn G, Abbeel P and Levine S (2021) Badgr: An autonomous self-supervised learning-based navigation system. *IEEE Robotics and Automation Letters* 6(2): 1312–1319. DOI:10.1109/LRA.2021.3057023.
- Karnan H, Warnell G, Xiao X and Stone P (2022) Voila: Visual-observation-only imitation learning for autonomous navigation. In: *2022 International Conference on Robotics and Automation (ICRA)*. pp. 2497–2503. DOI:10.1109/ICRA46639.2022.9812316.
- Keviczky T, Borrelli F and Balas G (2004) A study on decentralized receding horizon control for decoupled systems. In: *Proceedings of the 2004 American Control Conference*, volume 6. pp. 4921–4926 vol.6. DOI:10.23919/ACC.2004.1384629.
- Kingma DP and Ba J (2014) Adam: A method for stochastic optimization. *CoRR* abs/1412.6980.
- Li K, Xu Y, Wang J and Meng MQH (2019) Sarl: Deep reinforcement learning based human-aware navigation for mobile robot in indoor environments. In: *2019 IEEE International Conference on Robotics and Biomimetics (ROBIO)*. pp. 688–694. DOI:10.1109/ROBIO49542.2019.8961764.
- Liu L, Dugas D, Cesari G, Siegwart R and Dubé R (2020) Robot navigation in crowded environments using deep reinforcement learning. In: *2020 IEEE/RSJ International Conference on Intelligent Robots and Systems (IROS)*. pp. 5671–5677. DOI:10.1109/IROS45743.2020.9341540.
- Liu S, Chang P, Liang W, Chakraborty N and Driggs-Campbell K (2021) Decentralized structural-rnn for robot crowd navigation with deep reinforcement learning. In: *2021 IEEE International Conference on Robotics and Automation (ICRA)*. pp. 3517–3524. DOI:10.1109/ICRA48506.2021.9561595.
- Marcucci T, Petersen M, von Wrangel D and Tedrake R (2023) Motion planning around obstacles with convex optimization. *Science Robotics* 8(84): ead7843. DOI:10.1126/scirobotics.adf7843. URL <https://www.science.org/doi/abs/10.1126/scirobotics.adf7843>.
- Park J, Lee Y, Jang I and Kim HJ (2023) Dlsc: Distributed multi-agent trajectory planning in maze-like dynamic environments using linear safe corridor. *IEEE Transactions on Robotics* 39(5): 3739–3758. DOI:10.1109/TRO.2023.3279903.
- Paszke A, Gross S, Chintala S, Chanan G, Yang E, DeVito Z, Lin Z, Desmaison A, Antiga L and Lerer A (2017) Automatic differentiation in pytorch.
- Quigley M, Gerkey B, Conley K, Faust J, Foote T, Leibs J, Berger E, Wheeler R and Ng A (2009) Ros: an open-source robot operating system. In: *Proc. of the IEEE Intl. Conf. on Robotics and Automation (ICRA) Workshop on Open Source Robotics*. “Kobe, Japan”.
- Rusu AA, Vecerík M, Rothörl T, Heess NMO, Pascanu R and Hadsell R (2016) Sim-to-real robot learning from pixels with progressive nets. *ArXiv* abs/1610.04286. URL <https://api.semanticscholar.org/CorpusID:876231>.
- Schulman J, Moritz P, Levine S, Jordan MI and Abbeel P (2015) High-dimensional continuous control using generalized advantage estimation. *CoRR* abs/1506.02438. URL <https://api.semanticscholar.org/CorpusID:3075448>.
- Schulman J, Wolski F, Dhariwal P, Radford A and Klimov O (2017) Proximal policy optimization algorithms. *ArXiv* abs/1707.06347. URL <https://api.semanticscholar.org/CorpusID:28695052>.
- Shi Y, Yuan C, Tsitos AC, Cong L, Hadjar H, Chen Z and Zhang JW (2023) A sim-to-real learning-based framework for contact-rich assembly by utilizing cyclegan and force control. *IEEE Transactions on Cognitive and Developmental Systems* 15: 2144–2155. URL <https://api.semanticscholar.org/CorpusID:256180836>.
- Tang S, Thomas J and Kumar V (2018) Hold or take optimal plan (hoop): A quadratic programming approach to multi-robot trajectory generation. *The International Journal of Robotics Research* 37(9): 1062–1084. DOI:10.1177/0278364917741532. URL <https://doi.org/10.1177/0278364917741532>.
- Tobin J, Fong R, Ray A, Schneider J, Zaremba W and Abbeel P (2017) Domain randomization for transferring deep neural networks from simulation to the real world. In: *2017 IEEE/RSJ International Conference on Intelligent Robots and Systems (IROS)*. pp. 23–30. DOI:10.1109/IROS.2017.8202133.
- van den Berg J, Guy S, Lin M and Manocha D (2011) *Reciprocal n-Body Collision Avoidance*, volume 70. ISBN 978-3-642-19456-6, pp. 3–19. DOI:10.1007/978-3-642-19457-3_1.
- Xie P, Xia B, Hu A, Zhao Z, Meng L, Sun ZQ, Gao X, Wang J and Meng MQH (2024) Autonomous multiple-trolley collection system with nonholonomic robots: Design, control, and implementation. *Journal of Field Robotics* URL <https://doi.org/10.1002/rob.22395>.
- Xie X, Josifovski J, Malmir M and Knoll A (2023) Continual invariant image mapping from randomized simulations for sim2real transfer in robotic manipulation. URL <https://api.semanticscholar.org/CorpusID:259300488>.
- Xie Z and Dames P (2023) Drl-vo: Learning to navigate through crowded dynamic scenes using velocity obstacles. *IEEE Transactions on Robotics* 39(4): 2700–2719. DOI:10.1109/TRO.2023.3257549.
- Xue Y and Chen W (2024) Multi-agent deep reinforcement learning for uavs navigation in unknown complex environment. *IEEE Transactions on Intelligent Vehicles* 9(1): 2290–2303. DOI:10.1109/TIV.2023.3298292.
- Yan C, Qin J, Liu Q, Ma Q and Kang Y (2023) Mapless navigation with safety-enhanced imitation learning. *IEEE Transactions on Industrial Electronics* 70(7): 7073–7081. DOI:10.1109/TIE.2022.3203761.
- Yao S, Chen G, Pan L, Ma J, Ji J and Chen X (2020) Multi-robot collision avoidance with map-based deep reinforcement learning. In: *2020 IEEE 32nd International Conference on Tools with Artificial Intelligence (ICTAI)*. pp. 532–539. DOI:10.1109/ICTAI50040.2020.00088.
- Zhou X, Wang Z, Wen X, Zhu J, Xu C and Gao F (2021) Decentralized spatial-temporal trajectory planning for multi-copter swarms. *ArXiv* abs/2106.12481. URL <https://api.semanticscholar.org/CorpusID:235606313>.
- Zhu H, de Brito BF and Alonso-Mora J (2022) Decentralized probabilistic multi-robot collision avoidance using buffered uncertainty-aware voronoi cells. *Autonomous Robots* 46: 401–420. URL <https://api.semanticscholar.org/CorpusID:245854024>.
- Zhu K and Zhang T (2021) Deep reinforcement learning based mobile robot navigation: A review. *Tsinghua Science and Technology* 26(5): 674–691. DOI:10.26599/TST.2021.9010012.